Analysis and Validation of Multiphase CFD Predictions of SLS Ground System Loads Using Artemis I Launch Data

T. Rivord[1] and B. Williams.[2]
NASA Marshall Space Flight Center, Huntsville, AL

I. Introduction

The SLS mobile launcher (ML) is a crucial part of the Artemis mission ground systems, supporting the Space Launch System (SLS) rocket during assembly, transportation, and launch. The SLS propulsion system, consisting of four Aerojet-Rocketdyne RS-25 engines and two RSRMV solid rocket boosters (SRBs), generates a series of large magnitude pressure waves and launch acoustics during launch that the vehicle, and ground systems, must withstand. To reduce the magnitude of these pressure waves on the SLS vehicle, the ML is equipped with an ignition overpressure/sound suppression (IOP/SS) water system which injects water into the region of the RS-25 and RSRMV plumes in the mobile launcher hole (MLH). Images of the SLS being transported by the ML and the ML IOP/SS water system are provided in Fig. 1.

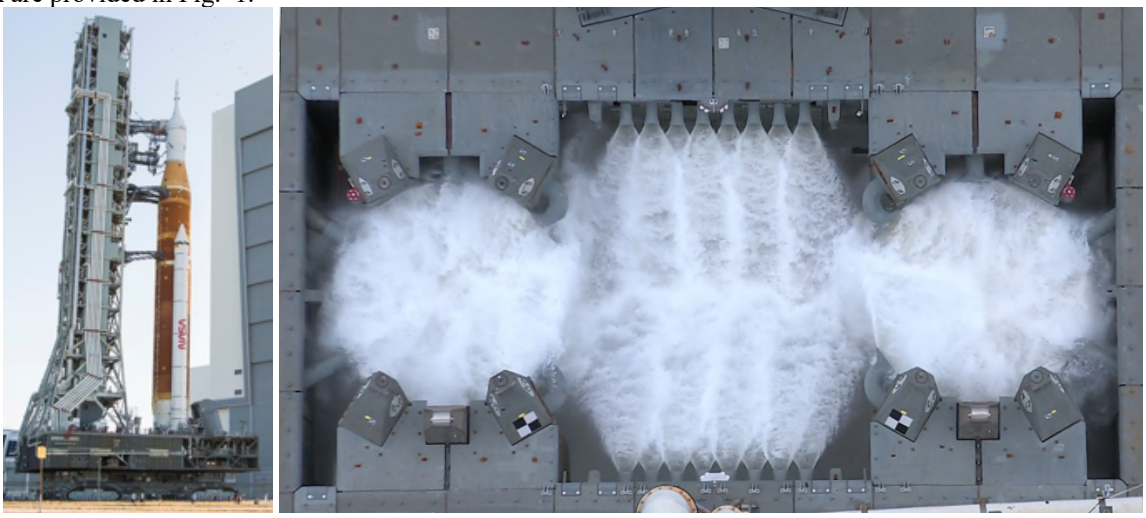

Fig. 1 SLS vehicle on the mobile launcher (left) and the mobile launcher IOP/SS water system (right).

While the intent of the SLS IOP/SS water system is to reduce the magnitude of the pressure waves generated by the SLS propulsion systems on the vehicle itself, the water can have the opposite effect (magnification, not suppression) on ground systems. One example of this magnification, increased pressures/loads on the SRB duct sidewalls, was identified during the Shuttle Program. The first Space Shuttle mission, STS-1, did not include any IOP mitigation water for the SRBs. Once IOP mitigation was added to the SRB ducts for all subsequent flights, markedly increased pressures were recorded on the SRB duct sidewalls as demonstrated in Fig. 2.

In addition to the IOP/SS water, the SLS launch pad at Kennedy Space Center's LC-39B contains a system to provide water for thermal protection of the main flame deflector (MFD) and the flame trench which are positioned below the ML. Similar to the Shuttle design, this water is injected from a series of large "mushroom cap" nozzles at the crest of the MFD as shown in Fig. 3 from video of a water flow test prior to Artemis I. The amount of water injected from the MFD crest nozzles is roughly equivalent to the IOP water injected in the MLH.

[1] CFD Analyst, NASA MSFC ER42, travis.a.rivord@nasa.gov
[2] CFD Team Lead, NASA MSFC ER42, brandon.williams@nasa.gov

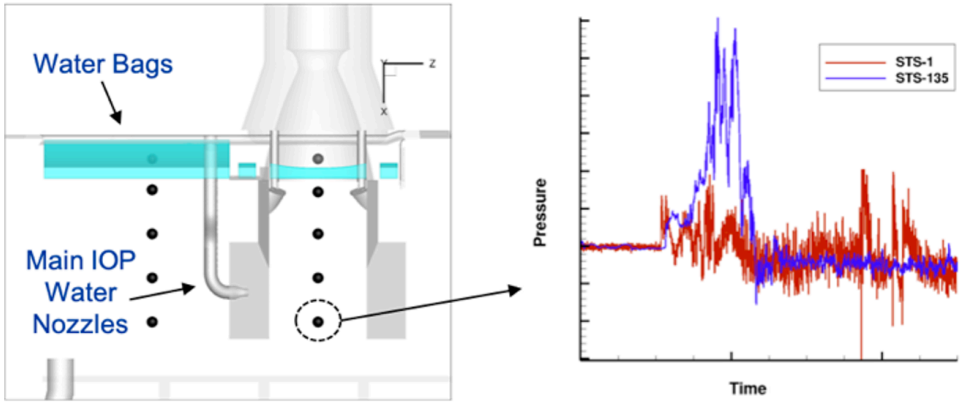

Fig. 2 Space Shuttle Mobile Launcher Hole increased wall pressures due to addition of sound suppression water.

Fig. 3 Water injected from the MFD crest at LC-39B during a water system flow test.

During the SRB ignition transient, the plume accelerates through the MLH and the flame trench as the motor chamber pressure rises, displacing the IOP/SS and MFD crest water and compressing air and vapor in its path. As a result, large magnitude, relatively low frequency overpressure waves are generated. The portion of the waves that propagate upward through the MLH are called ignition overpressure (IOP), while the waves that travel outward through the flame trench are known as duct overpressure (DOP). Besides direct plume impingement as the vehicle lifts off, the DOP waves create the greatest launch-induced loads on the ground structures because the pressure is distributed over the large surface area under the ML. The Artemis I DOP wave can be visualized from high speed video frames in Fig. 4 by tracking the disturbances in the vapor below the ML and rapid expansion as it exits the flame trench.

The influence of the IOP/SS and MFD crest water on the DOP wave and the magnification of the pressures/loads on the underside of the ML underside was identified during the SLS Scale Model Acoustic Test (SMAT) series. SMAT tests were conducted both with and without water to measure the water mitigation effects on the vehicle. Pressure probes on the ML underside recorded as much as 4X higher pressures for tests with water compared to those without, as demonstrated by Fig. 5 [1].

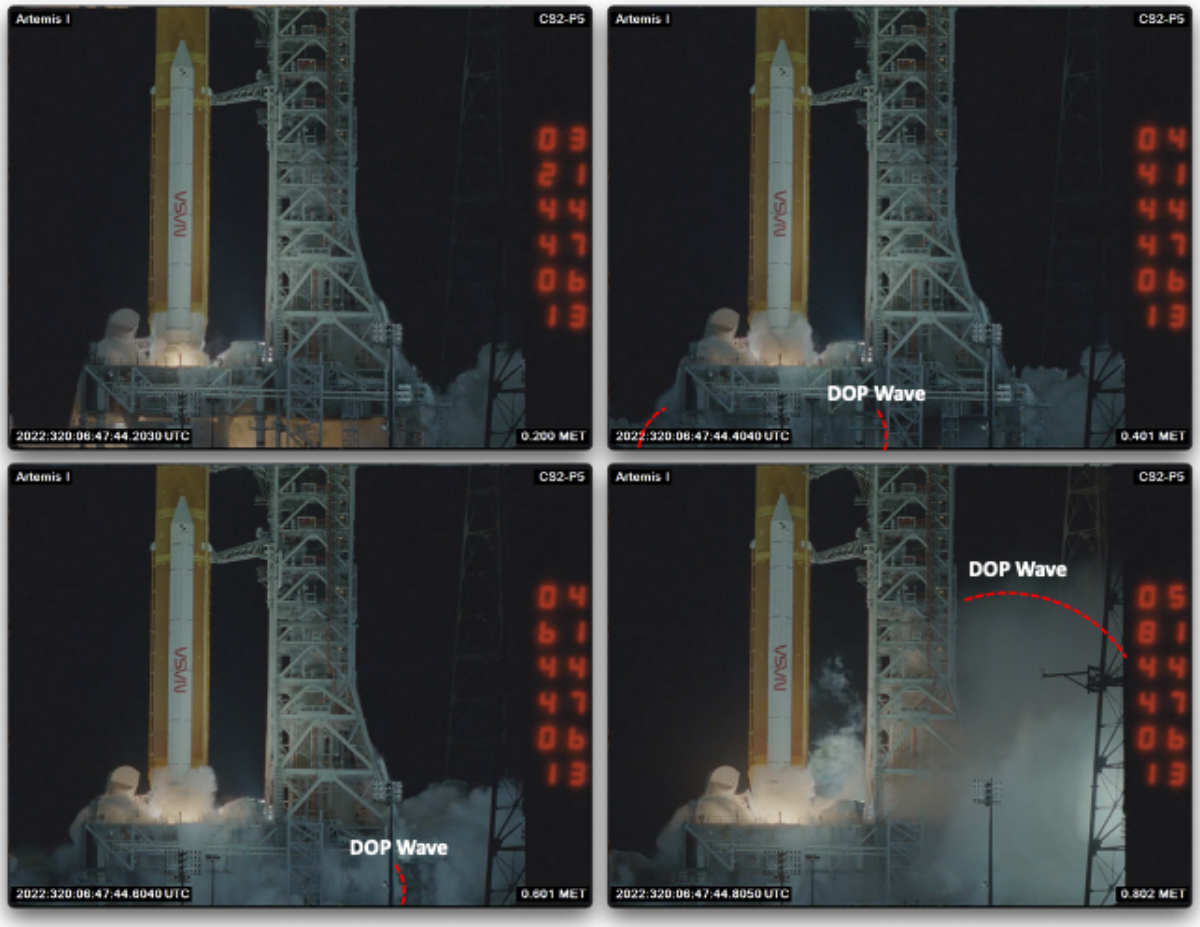

Fig. 4 Artemis I high speed video (images.nasa.gov) showing the DOP wave traverse and exit the flame trench.

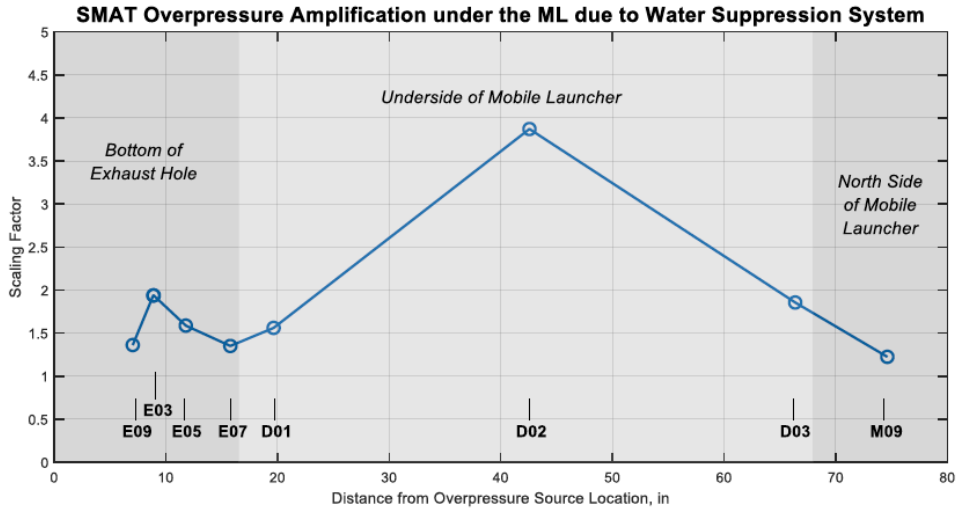

Fig. 5 SMAT Overpressure Amplification under the ML due to the IOP/SS Water System.

Both the elevated MLH sidewall and ML underside pressures were expected to occur during the SLS flight, though there was uncertainty regarding the timing and magnitude of the elevated pressures due to configuration and scaling

differences from SMAT. Since no integrated system test would occur prior the Artemis I SLS flight, computational fluid dynamics (CFD) was relied upon to inform the program on the ground environment.

Prior to the Artemis I flight, five CFD predictions of the multiphase SLS launch environment were executed and used to support aspects of the SLS program including but not limited to RS-25 lead hydrogen burn-off igniters (HBOIs) operation, water system design, debris transport, and environment development. However, validation of these CFD tools on the launch environment were limited to individual SLS system tests [2]. Only one of these five simulations included the main flame deflector MFD crest water within the flame trench. As the crest water is expected to have a first order effect on the launch environment in the flame trench, only this simulation is used to study the launch environment experienced by the ground systems.

Following the November 2022 Artemis I SLS flight, comparisons of the CFD prediction to the flight test data was made. The purpose of this paper is to present validation of the multiphase CFD simulation for launch environment prediction with a focus on the magnified environment experienced by the ground systems. Examination of the validated simulation flowfields provides a deeper understanding of multiphase environments, which can be used to improve environment development and support future launch vehicles.

II. Computational Model

The SLS ignition sequence occurs in three distinct steps. First, the IOP/SS water is activated and reaches a steady state prior to RS-25 ignition. Next, approximately six seconds prior to T0, the RS-25 engines ignite, then reach 100% rated power level (RPL) after four seconds. Lastly, the SRB ignition is initiated at T0, though it takes approximately 0.1 seconds for the igniter shock to travel the length of the booster.

The CFD simulation was conducted in three similar phases to mimic the physical launch sequence. First, the IOP/SS water was developed to a quasi-steady state. Next, the RS-25 engines were activated and ramped to 100% RPL and lastly, the SRB was activated. While all three phases of the launch environment were simulated, only the final portion, the SRB ignition transient, is examined presently.

The SLS multiphase CFD simulation was executed with water flowrates based on the Integrated System Verification and Validation 14 (ISVV-14) test series of the IOP/SS system at Kennedy Space Center (KSC), which is considered a lower bound on the flight water flowrates. The Demonstration Motor 1 (DM-1) high propellant mean bulk temperatures (PMBT) SRB transient was used, which closely resembles the flight temperature.

A. Computational Domain and Mesh

The computational geometry was generated using a combination of the SLS geometry from [3], the verified CAD model of the ML [4], and the IOP/SS geometry provided by Exploration Ground Systems (EGS) [5]. On the ML, only those features expected to affect the IOP/SS water flow and initial plume environment were retained, and many of those were simplified. Only the aft portion of the SLS vehicle was modeled as only this portion will interact with the IOP/SS water. The flame trench contains a truncated, idealized model of the rectangular duct, with simplified versions of the side deflectors and the main flame deflector (MFD) which do not include the details of the support structures on the backside of the deflectors nor the segments of steel plate that form the MFD surface. These geometry modifications were made to reduce the mesh size and complexity. To further reduce the computational expense of the simulation, a symmetry boundary condition was placed at the vehicle centerline. Though the presence of the symmetry plane is not thought to significantly affect the results from the present simulations, this needs to be investigated further. The final computational domain and geometry for the SLS multiphase launch environment simulation is provided in Fig. 6.

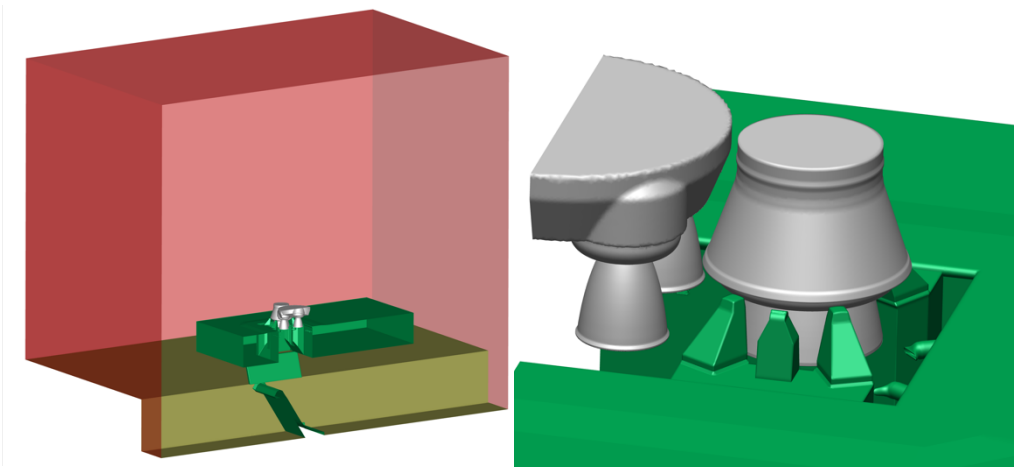

Fig. 6 Simulation computational domain and geometry.

The distribution of cells in the computational mesh is demonstrated by Fig. 7, which shows the mesh characteristic length scale, calculated as the cube-root of the cell volume, on vertical cutting planes through the vehicle centerline and flame trench. As the focus of the simulation was on the interaction of the SLS rocket plumes and IOP/SS water, the bulk of the mesh density was targeted to capture the water features and interactions in those regions.

The mesh edge length within the MLH is targeted at 2" and grows prism layers on all solid walls to enable resolution of a viscous boundary layer. Resolution within the trench is maintained at 6" to target capturing the IOP and DOP waves expected to form. Regions outside of the MLH and trench grow rapidly to reduce mesh cell count and dissipate pressure waves prior to hitting farfield boundaries. The final mesh cell count is 86 million.

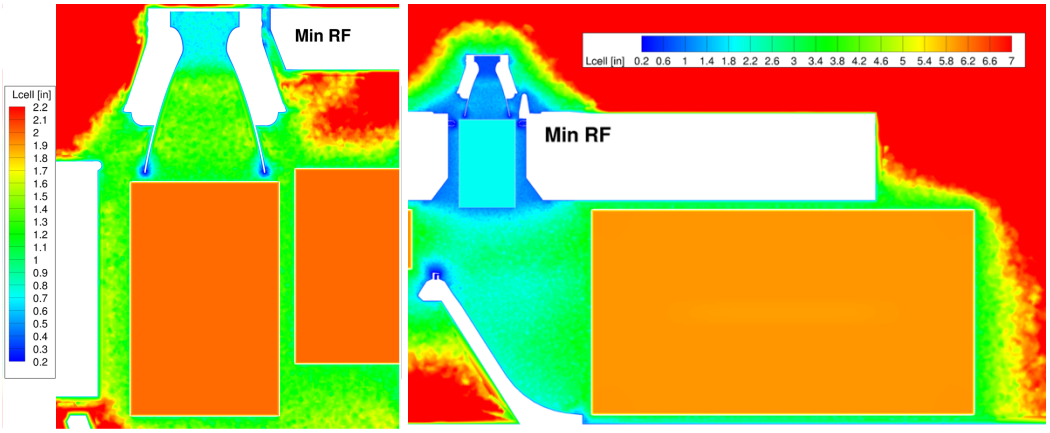

Fig. 7 Characteristic cell lengths on cutting planes through the vehicle centerline (left) and flame trench (right).

B. Computational Settings

The SLS multiphase CFD simulation was executed with the density-based Loci/CHEM-Real Fluid (RF) CFD solver. In the Loci/CHEM-RF model, the liquid essentially acts as a very dense gas species with appropriate thermodynamic and phase change properties; the liquid phase is governed by a stiffened (e.g., barytropic) or tabular equation of state, and multiple models are available for cavitation and evaporation. The Loci/CHEM-RF model does not explicitly track or model the details of the gas-liquid interface. Because of this, surface tension is not included, droplets and ligaments of liquid are not resolved, and the liquid in interfacial regions is allowed to mix and diffuse in a non-physical manner. For example, were a droplet initialized in a quiescent domain free of body forces, it would eventually diffuse to fill the domain.

While the RF model was not intended for this type of launchpad application, it has shown reasonable results in certain problems where interface details are not important and timescales of numerical diffusion are much longer than fluid convective timescales. A log scale slice of density through the SLS SRB centerline is presented in Fig. 8 to

demonstrate the RF model's representation of water. The RF model captures the total water mass and general location of the water, but neither the density of liquid water nor discrete drops of water.

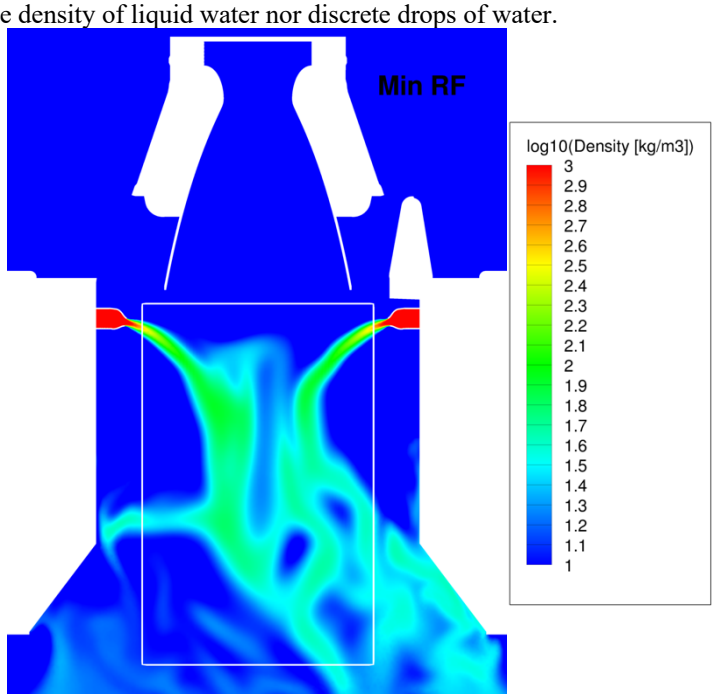

Fig. 8 Log10 scale of density for the Loci/CHEM-RF simulation of the SLS water system.

The simulation was executed with second order spatial and second order temporal accuracy. The inviscid flux scheme applied is the HLLE (Harten-Lax-van Leer-Einfeldt) flux scheme formulated with Chorin-Turkel (CT) local preconditioning scheme. Generally, the HLLE flux scheme is regarded as dissipative, at least compared to the stiffer Roe flux scheme. The simulation was executed with a hybrid Reynold-averaged Navier-Stokes (RANS)-large eddy simulation (LES) turbulence model. All walls were set to viscous walls. The prism layer on each surface was resolved sufficiently to capture the boundary layer without the use of wall functions.

III. Analysis

One instance where the addition of IOP/SS water magnifies the pressure environment is on the MLH sidewalls. It was known from the Shuttle Program that the addition of water under the SRB magnified pressures experienced on the surrounding walls, as demonstrated in Fig. 2. Preliminary multiphase CFD simulations of the Shuttle launch configuration indicated this increased pressure was due to the SRB plume impinging on the walls after being diverted outwards radially by the water. For Shuttle, the amplification of the sidewall pressure primarily occurred near the vertical location of the main IOP water nozzles, where the majority of the water in the MLH was injected.

Although the total IOP water flow rates into the MLH under the SRBs are similar in SLS versus Shuttle, the SLS IOP water system design is significantly different. The clean sheet design of the ML for SLS allowed designers to move the water closer to the nozzle exit. This would provide the desired acoustic mitigation without the need for the water bags that were hung across the SRB holes in the Shuttle mobile launcher platform (MLP) (see Fig. 2). The 6 SLS IOP nozzles under each SRB (see Fig. 1) are aimed at the centerline of the SRB, where the opposing water jets meet and form a dense column of water directly below the SRB nozzle, as illustrated in Fig. 8. This column of water creates a barrier for the SRB plume during the ignition transient until the plume can either displace or evaporate the water. Because the SLS IOP water is all injected high in the MLH, there is comparatively more water near the nozzle exit plane in SLS than Shuttle. As shown in Fig. 9, the quantity of water in the projected volume of the SRB nozzle in the upper half of the MLH is 3-4X greater in the SLS configuration, and does not reach parity until the bottom. As a result, it may be expected that the plume-water interaction during SRB ignition could be stronger for SLS, and consequently the sidewall loads could be larger than those observed during Shuttle.

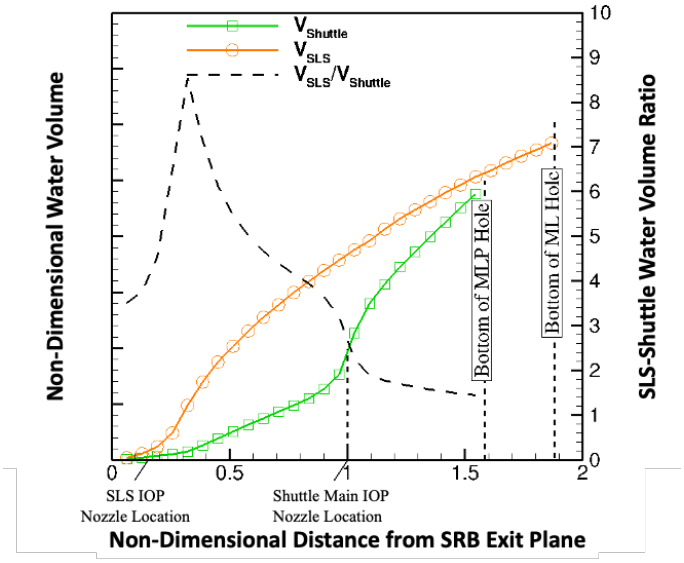

Fig. 9 Cumulative IOP water volume below the SRB nozzle.

Pressure data, with no filtering applied, along the MLH side wall is provided for a dry (i.e., no water) CFD simulation, Artemis I flight, and the wet CFD simulation in Fig. 10. All probes provided are from the EI-LIE-### set of pressure transducer measurements from the Artemis I flight; the names have been shortened to P## here. All plots have the same X and Y-axis ranges to enable comparisons. The flight and wet CFD data, both of which include water, have significantly higher pressures (greater than 5X) compared to the dry CFD. For reference, the magnification of sidewall pressures due to the addition of water observed during the Shuttle Program (Fig. 2) was 3X. Additionally, the SLS flight sidewall pressures were approximately 2X the magnitude of those observed during Shuttle. This aligns with the above expectation that SLS, which has a higher concentration of water close to the SRB exit plane, would experience higher magnitude sidewall impingement pressures than Shuttle.

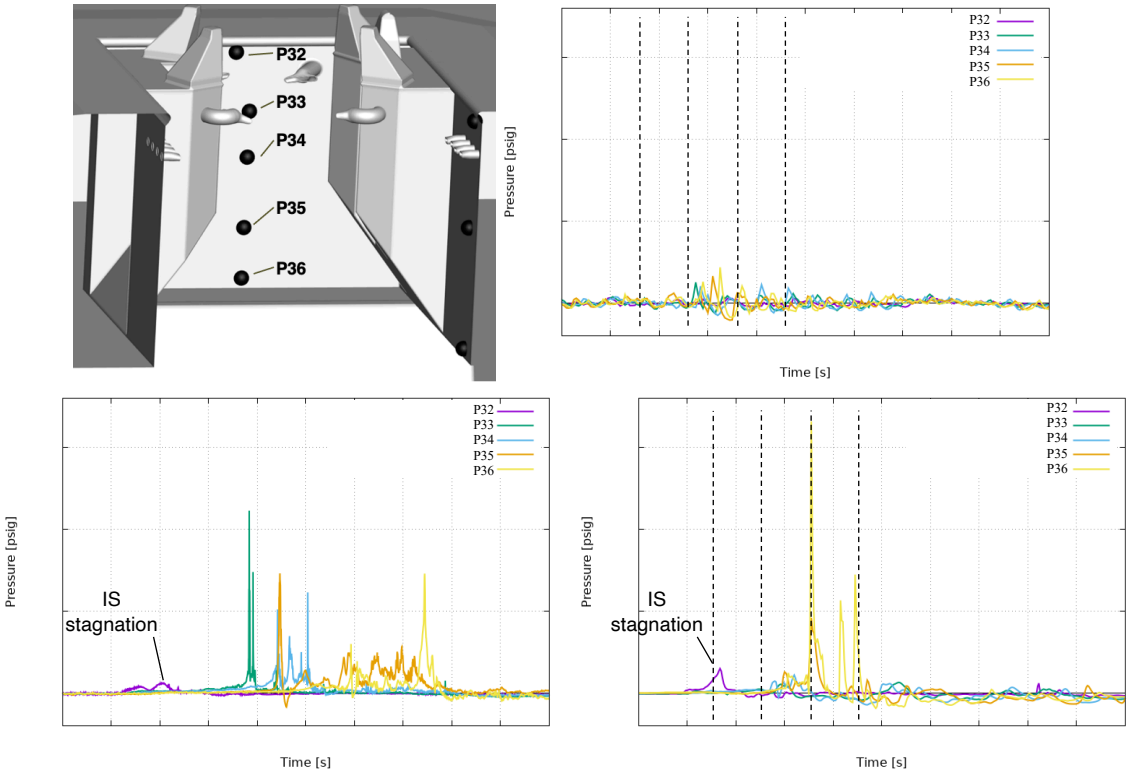

Fig. 10 Pressure probes along the MLH west sidewall for dry CFD (top), Artemis I (left), and wet CFD (right). Vertical lines on the CFD dataset correspond to times provided in Fig. 11.

The evolution of the CFD flowfields are provided in Fig. 11 with the dry CFD presented in the left two images and the wet CFD presented in the right two images. The rainbow contour of each set is velocity magnitude while the cool-warm contour of each set is gauge pressure centered at 0 psig. The wet CFD solutions have a density iso-line representing the water location. The times presented are equivalent between the two simulations and provided at equal time increments, which correspond to the vertical lines in Fig. 10.

In the dry simulation, the SRB plume emerges from the nozzle and advects through the MLH as a contiguous entity, not making contact with the MLH walls. The lack of direct plume impingement explains the relatively low magnitude pressures in the dry CFD data.

In the wet simulation, the SRB plume emerges from the nozzle and encounters the water in the MLH. The water covering the MLH under the SRB is primarily in a column at the SRB centerline with thinner regions outboard from that centerline. When the SRB igniter shock (IS) flow, which precedes the hot combustion gases of the plume, first encounters the water, it does not have enough momentum to immediately displace the water covering the MLH. Instead, the IS flow is redirected outwards radially from the SRB centerline. When this outward IS flow impinges on the MLH wall, as seen in the first frame of Fig. 11, it causes the first pressure rise at P32 in the wet CFD data. As the SRB plume continues to advect into the MLH, it first pushes through the thinner outboard regions of water and slowly advects the column of water at the centerline. This interaction redirects the SRB plume outward in all directions from the centerline. Elevated pressures are observed when the redirected plume impinges on the sidewalls. Probes P35 and P36 in the wet CFD data both experience pressure rises at nearly the same time. This is because the plume impinges over a broad region encompassing both probe locations. The probes higher up in the MLH, P32, P33, and P34, do not exhibit such high magnitude pressures because the SRB plume impinges below them.

Focusing now on the flight data, the outward IS flow stagnation on the sidewall is observed as the first pressure rise at P32. The wet CFD simulation predicts that this impingement occurs earlier and with a larger magnitude compared to flight. The MLH sidewall pressurization caused by SRB plume impingement begins at P33, just below the SRB water sheets, then travels downwards in time. The wet CFD simulation predicts that the first impingement occurs lower in the MLH compared to flight. Additionally, the wet CFD predicts higher magnitude pressurizations suggesting that the predicted impingement pressure magnitudes are likely overpredicted due to insufficient numerical convergence. Though the wet CFD simulation does not exactly match the flight data, it does successfully predict that the SRB plume is redirected outwards by the column of water at the SRB centerline causing large-magnitude pressurizations on the MLH sidewalls.

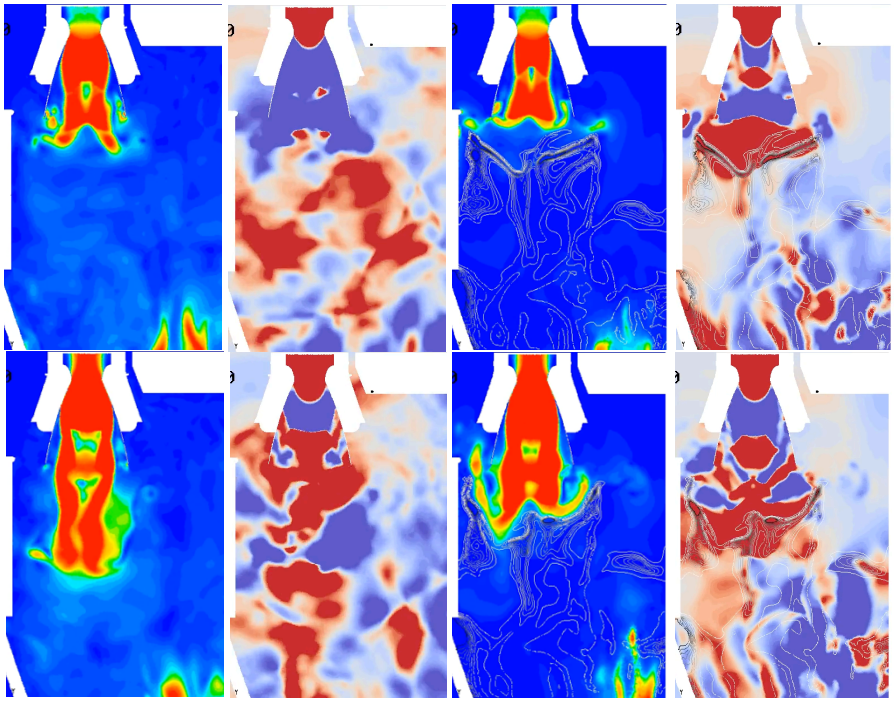

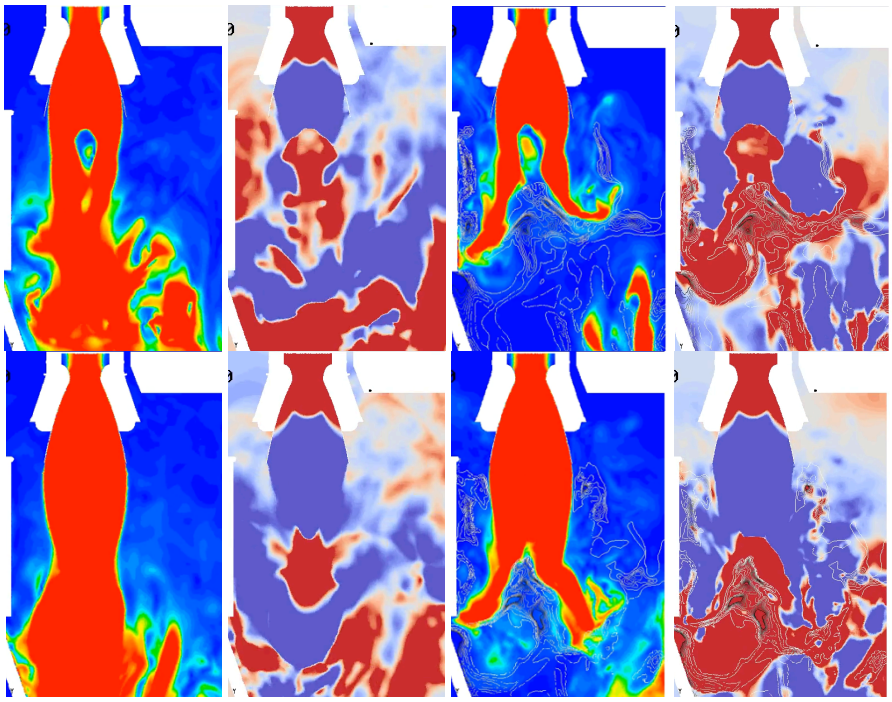

Fig. 11 Progression of CFD flowfields during high MLH sidewall pressures. Left two images are dry CFD, right two are wet CFD. Velocity (left) and pressure (right) contours a density iso-line representing the water.

Another example of the IOP/SS water amplifying pressures experienced on ground systems is the underside of the mobile launcher (ML). As described previously, it was found during the subscale SMAT testing that the addition of water resulted in pressures as much as four times higher as those without water [1]. Pressure data, with no filtering applied, along the underside of the ML is provided for an equivalent dry CFD simulation, Artemis I flight, and the wet CFD simulation in Fig. 12. All probes provided are from the EI-LIE-### set of pressure transducer measurements from the Artemis I flight, though the names have been shortened to P##. All plots have the same X and Y-axis ranges to enable comparisons. The flight and wet CFD data, both of which include water, have significantly higher pressures (greater than 2X) compared to the dry CFD without the effects of water. This confirms that the elevated ML underside increased pressures observed during the SMAT testing also occurs with the full scale SLS configuration.

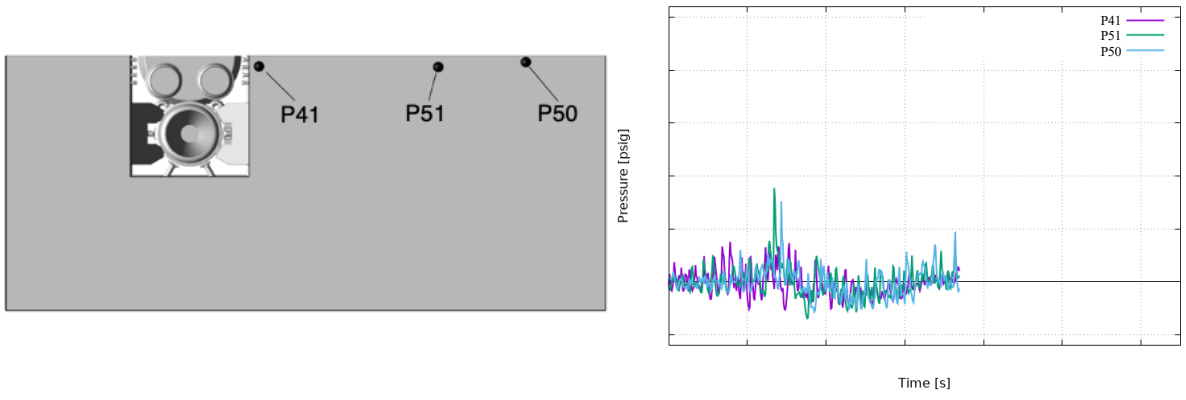

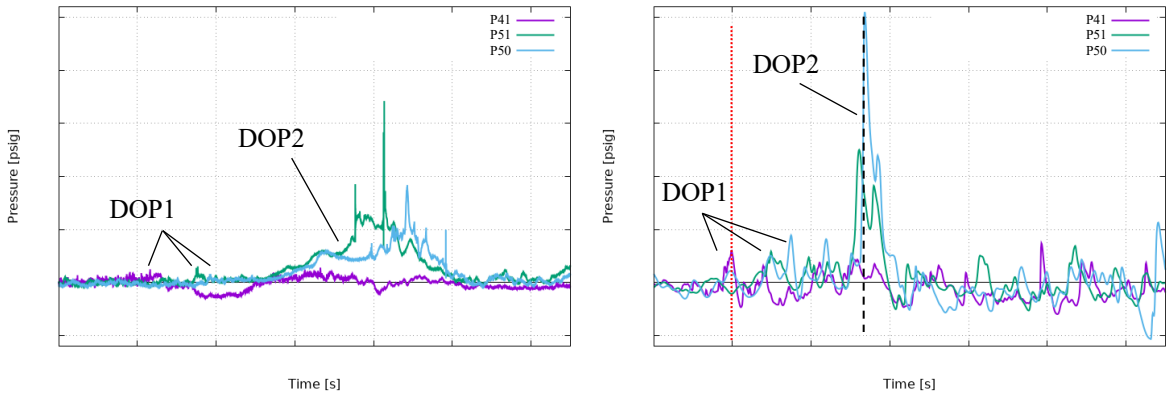

Fig. 12 Pressure probes along mobile launcher underside for dry CFD (top), Artemis I (left), and wet CFD (right). Vertical lines on the CFD dataset correspond to times provided in Fig. 14.

The maximum ML underside pressure in the dry (left) and wet (middle) simulations are provided in Fig. 13 along with the resulting amplification factor (right). The pressure contours are not selected to highlight the maximum pressure values, but rather the general change in pressure values due to the addition of water. The amplification factor is simply the maximum wet pressure divided by the maximum dry pressure at each node in the ML surface mesh. It can be seen that the highest wet/dry amplification factors are confined towards the ML centerline and decay laterally outward from the flame trench. Additionally, the highest amplification factor is concentrated towards the exit of the flame trench, which corresponds to the regions of the most rapid expansion of visible vapor in Fig. 4. Viewing the ML underside pressure contours for both the dry and wet simulations demonstrates that the amplification observed at probes P51 and P50 are not localized, but broader impacts due to the addition of water.

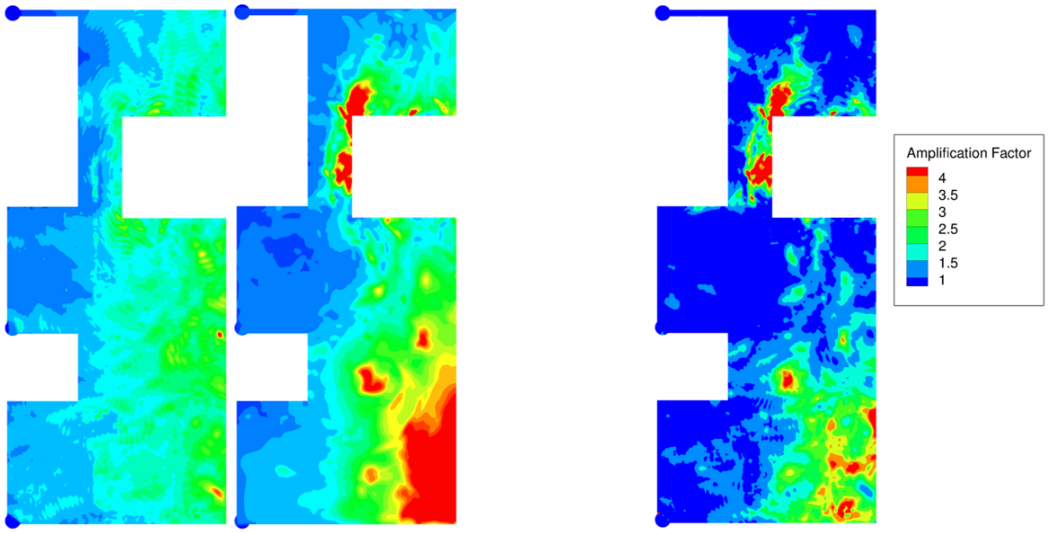

Fig. 13 Maximum ML underside pressure for the dry (left) and wet (middle) CFD and the resulting amplification factor (right).

The evolution of the wet CFD flowfield is provided in Fig. 14 with time increasing from left to right, top to bottom. The slice is through the SRB centerline displaying gauge pressure (blue low, red high) and a density iso-line representing the water. It should be noted that this plane is provided through the SRB centerline and not through the actual probe locations at the center of the flame trench. The bottom left image corresponds to the dotted vertical red line in Fig. 12.

This sequence shows the pressure source formed by the SRB plume compressing the ambient air within the confined MLH duct. This source releases as it travels from the confined MLH into the larger trench volume. The downward-traveling portion of this wave is referred to as DOP1. As the DOP1 wave diffracts into the flame trench, it passes P41 and causes the pressure rise observed in Fig. 12. This DOP1 pressure wave then passes the P51 and P50

locations as it propagates the length of the trench. The flight data exhibits a similar pressure rise as the CFD, though the CFD is slightly earlier and approximately 2X the magnitude of the flight data.

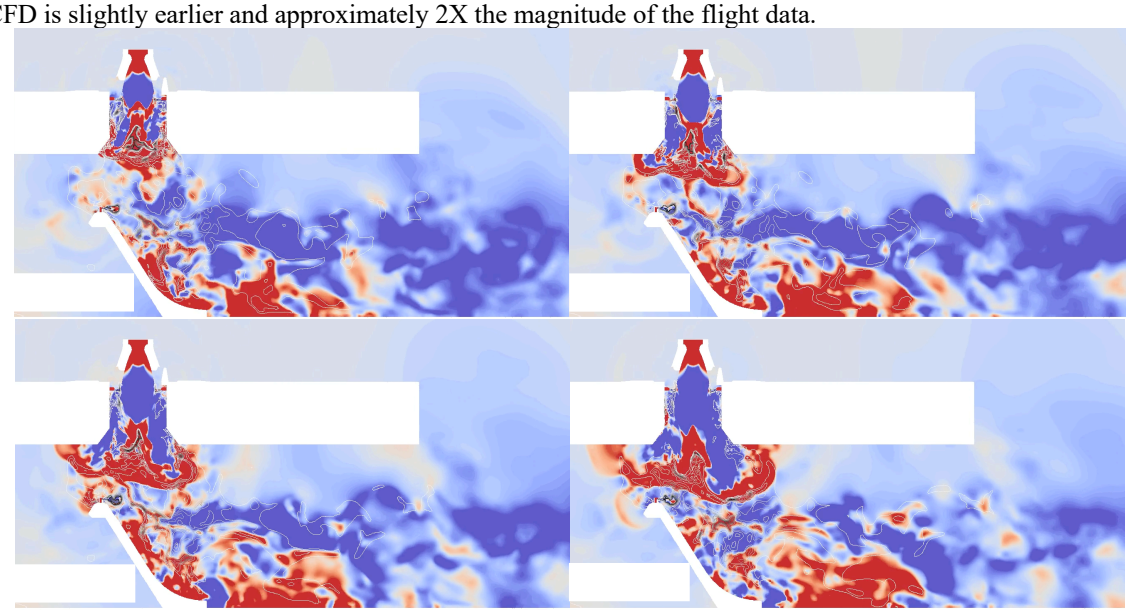

Fig. 14 Progression of DOP1 in the trench for the wet CFD flowfield.

Another sequence of pressure slices in Fig. 15 illustrates the evolution of the DOP2 wave. Note that the time increment between frames is slightly longer than in Fig. 14. The sequence through the first three rows shows the SRB plume pushing through the water and impinging on the main flame deflector (MFD). In the subsequent images, it can be observed that the inertia of the water injected from the MFD crest into the trench delays the advection of the plume. This results in pressure building behind that water blockage, forming the DOP2 source. The plume in the pressurized region between the trench floor and water eventually lofts the water upwards and downstream, at which point the pressure source releases creating the DOP2 wave. The DOP2 wave travels mostly upwards and downstream to impact the underside of the ML, which corresponds to the last image in Fig. 15 and the black dashed line in Fig. 12. The wet CFD pressure data indicates that the DOP2 wave impacts P51 just before P50. The DOP2 wave also travels upstream to impact P41, though with a much lower magnitude than P51 and P50.

The wet CFD simulation agrees with the trends observed in the flight data. P41 experiences significantly lower pressurization compared to the probes further downstream. Additionally, P51 experiences elevated pressures just prior to P50. The primary difference between the CFD and flight data is the magnitude and timing of the pressurization predicted. The CFD pressurization at P51 and P50 occurs earlier, with four times higher magnitude, and has a shorter duration than the flight data. Although the source of the timing and duration differences cannot yet be explained, the higher pressure magnitude of the DOP wave can be attributed to known deficiencies in the RF model for this type of problem. In a non-published CFD study of a different launch vehicle and pad configuration, comparisons between the RF model, a higher fidelity volume of fluid (VoF) model, and flight data yielded similar results. The RF model predicts significantly more blockage of the plume, and consequently higher pressures, within the trench due to the diffuse and non-physical nature of the liquid water model. Instead of the water breaking up into smaller, discrete volumes of droplets and ligaments with some space between them, the RF water creates a continuous field of higher density fluid in the trench. This restricts the motion of the plume and prevents the relief of the pressure that builds up. Though the Loci/CHEM-RF simulation does not exactly match the flight data, it does successfully predict that the water in the trench results in large-magnitude pressurizations on the underside of the ML.

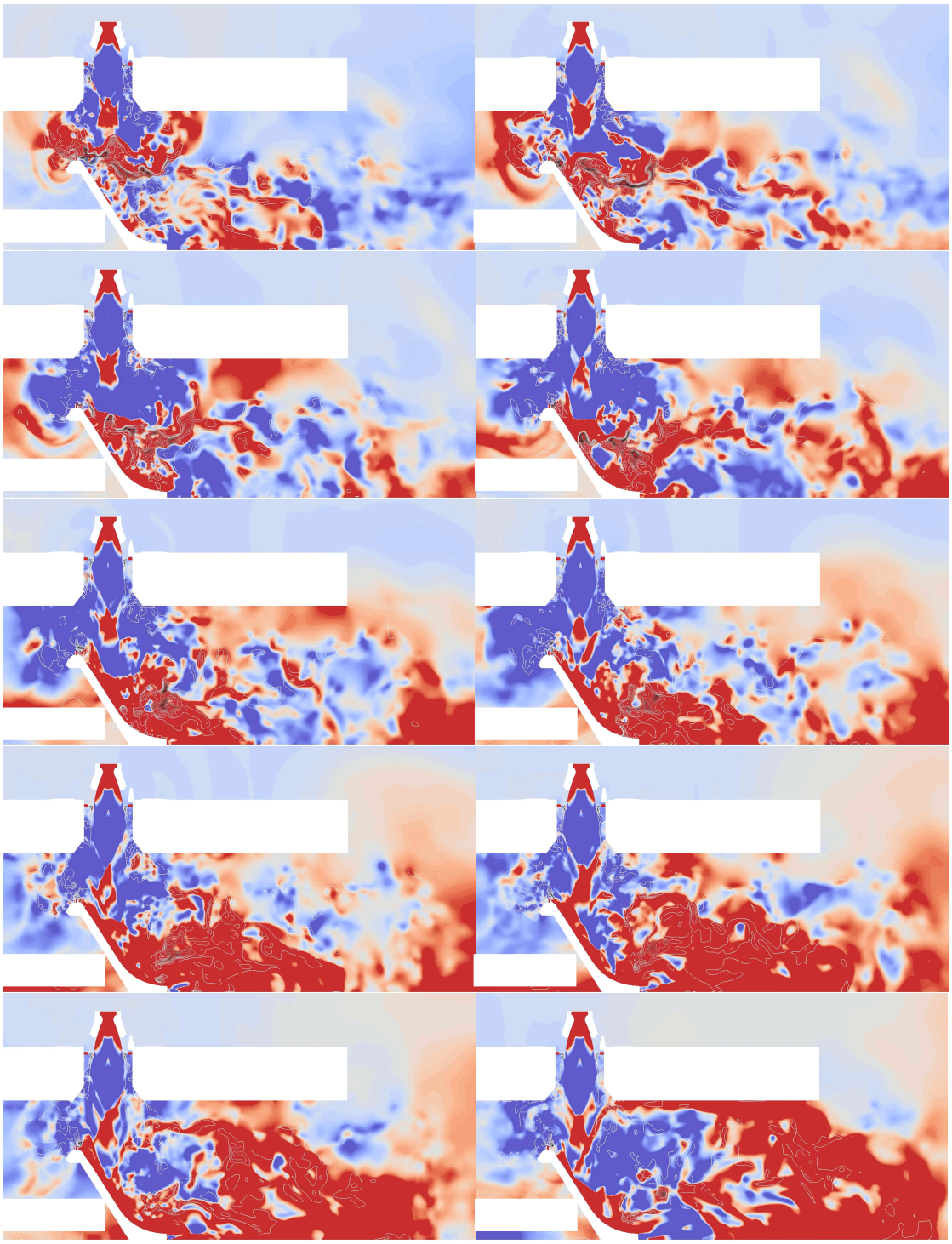

Fig. 15 Progression of DOP2 in the trench for the wet CFD flowfield.

IV. Conclusion

While the SLS IOP/SS water system effectively reduces the loading on the vehicle due to the liftoff pressure and acoustic environment, it has the unintended effect of amplifying the loads experienced by the ground systems, including the mobile launcher (ML). The Shuttle Program and subscale SMAT test series demonstrated that the MLH sidewall and ML underside pressures were amplified due to the addition of water, though the extent of magnification

expected for the SLS launch configuration was unknown due to lack of integrated SLS system tests. Several multiphase CFD simulations were executed with the Loci/CHEM-Real Fluids (RF) solver to support the SLS Program prior to launch. One simulation was suited to predict the ground system pressure amplification, which was compared to the November 2022 Artemis I SLS flight data.

The CFD simulation was found to successfully predict the amplification of MLH sidewall pressures as a result of the dense column of water at the SRB centerline turning the plume outboard to impinge on the walls. The CFD was also found to successfully predict the amplification of ML underside pressures due to water blockage in the flame trench. Though there were some discrepancies in the timing and magnitude of the pressurizations, significant insight into the physics occurring during the SLS launch was gained by examining the CFD flowfield. The results of this analysis substantiate the successful validation of Loci/CHEM-RF CFD solver for prediction of the complex multiphase launch environment ground systems experience and provide confidence in the application of this tool to future variants of the SLS vehicle as well as other heavy lift launch vehicles and launch pad designs.

References

[1] Casiano, M., Liu, T., Rivord, T., and Williams, B. ER42 (20-057), "Predicted Loads for the Underside of Mobile Launcher 2 Due to Space Launch System Booster Ignition." Huntsville, AL, 15 June 2020.

[2] Rivord, T. and Williams, B., "Validation of SLS Launchpad Water and Plume-water Induced Side Loads," *JANNAF*, June 2022.

[3] L. Strutzenberg. ER42 (14-133), "SLS DAC3 Geometry for CFD: RS-25 and Booster Nozzle Internal." Huntsville, AL, December 2014.

[4] L. Strutzenberg. ER42 (14-037), "Delivered SLS DAC3 Integrated Pad ML 10005 Geometry for CFD Part 1: Deck Plume Impingement." Huntsville, AL, December 2014.

[5] T. Drake., "Transmittal Memorandum-SBU and RFTU, IOP/SS Water Flow Rate Schedule Interdependency 1032: Water Nozzle CAD geometry; Interdependency 1033.", 15 March 2017.